Precision Energy Measurements with the RD52 Fiber Calorimeter

Sehwook Lee (Texas Tech University) on behalf of the RD52 collaboration

***Abstract*—The RD52 calorimeter measures the electromagnetic fraction of hadron showers in every event through simultaneous detection of the Cerenkov and scintillation light. This makes it possible to eliminate the main factor that prohibits precision energy measurements for hadrons. In Nov. 2012, the RD52 (DREAM) collaboration tested the performance of the new fiber calorimeter for the first time with high energy particles at the CERN SPS. The results presented here concern the performance characteristics for electrons and pions, as well as the identification of electrons in this longitudinally unsegmented calorimeter.**

I. Introduction

THE CALORIMETER is the most important detector in modern high energy particle physics experiments. In such experiments, the basic information is the measurement of the energy and momentum of the particles as well as particle identification. In these measurements, the calorimeter is crucial, not only for measuring the particle energy, but also to identify the electromagnetic particles and hadrons. Measurement of particle energy with excellent resolution is an essential requirement for high quality particle physics experiments just as gamma ray spectroscopy with high-purity Germanium crystal detectors opened a new era of nuclear physics. At a linear e^+e^- collider, whose construction has become more likely as a result of the recent Higgs discovery, hadronically decaying W's and Z's have to be measured as well as electrons and gamma's. The main obstacle that limits high precision energy measurements for single hadrons and jets is formed by the fluctuations of the electromagnetic component (f_{em}) in hadron showers. One solution to eliminate these fluctuations pursued by the RD52 (DREAM) project is to measure the electromagnetic component event by event. This method has been proven to eliminate the fluctuations of the em shower component and achieve high precision energy measurements for hadrons. This method offers the same advantages as compensating calorimeters (e/h=1) without the limitations of the latter devices. The interest in applying this technique is growing, for example, in upgrades of the CMS Forward Hadron calorimeter, in experiments at future colliders and in experiments in space. In Nov. 2012, we carried out measurements with the new RD52 fiber calorimeter at CERN. In this 2013 IEEE conference, we present results of these tests on:

1 The electromagnetic performance.
2 The hadronic performance.
3 Particle identification in the longitudinally unsegmented calorimeter.

II. Experimental setup and the RD52 fiber calorimeter

Fig. 1a shows the experimental setup for the Nov. 2012 beam test which was conducted in the H8C area at the CERN SPS. Wire chambers, trigger counters and a preshower detector were installed between the beam pipe (which is in the lower left corner) and the RD52 calorimeter contained in the rectangular box. This box houses 9 Pb-fiber and 2 Cu-fiber modules. The length of each module is 2.5 m (10 λ_{int}), and

(a) (b)

Fig. 1. The experimental setup during Nov. 2012 test beam in the H8C area of SPS at CERN (a), and the tower map of the Pb-fiber and Cu-fiber calorimeters (b).

its cross section is 92×92 mm^2. Each module is divided into 4 towers, so each tower measures $46 \times 46 \times 2500$ mm^3. The nine Pb-fiber modules were assembled as 3×3 matrix, and the two Cu-fiber modules were placed on top of the 3×3 matrix (Fig. 1b). Fig. 1b shows that the towers in the Pb-fiber modules form a central cell (T15) surrounded by three rings. In the tests, either T15 or Al2 was exposed to the electromagnetic or hadronic particle beams. Fig. 1a also shows 20 leakage counters, which were installed around the fiber calorimeters to detect shower leakage. A scintillator plate installed right behind the fiber calorimeters was used to eliminate hadron and muon contamination in the electron beam. A scintillator paddle placed 25 m downstream behind additional absorbers, was used to identify muons.

Fig. 2 shows the basic structures of the Pb-fiber (a) and Cu-fiber (b) modules. For the Pb-fiber module, we made grooves on both sides of a Pb plate, and put scintillation and Čerenkov fibers in alternating rows of grooves. The copper plates had grooves on one side only, and scintillation and Čerenkov fibers were embedded alternately in each row.

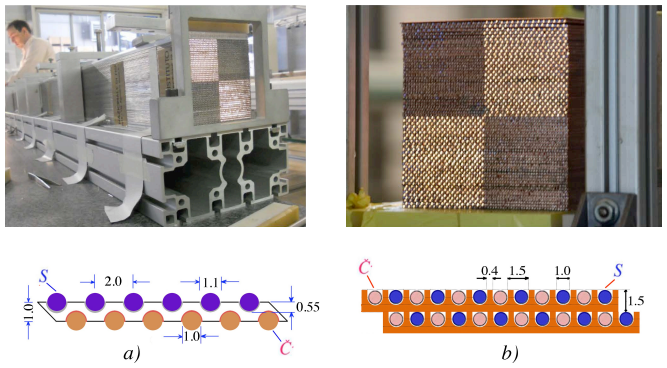

Fig. 2. Pictures and basic structures of the Pb-fiber (a) and Cu-fiber (b) modules.

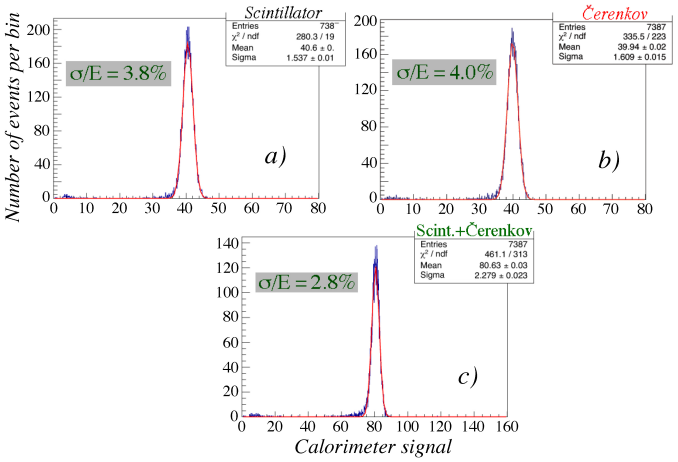

Fig. 3. Signal distributions of the scintillator (a), Čerenkov channels (b), and the distribution of the combination of both types of signals (c) for 40 GeV electrons in the Cu-fiber calorimeter.

III. Experimental Results

A. The electromagnetic performance

Fig. 3 shows the response functions of the Cu-fiber calorimeter to 40 GeV electrons. Each tower of the RD52 fiber calorimeter has two independent channels, which produce the scintillation and Čerenkov signals. These two channels were calibrated with a 20 GeV electron beam sent into each tower. Fig. 3a and b show the signal distributions of the sums of the scintillator and Čerenkov channels, respectively, for 40 GeV electrons. The energy resolutions obtained for these individual signals are 3.8% and 4.0%. The Cu/Scintillating-fiber and Cu/Čerenkov-fiber structures sample the showers independently. Therefore, the resolution improves when these two types of signals are combined. Fig. 3c shows the distribution of the combined signals, and the energy resolution becomes 2.8%.

Fig. 4 shows the em energy resolution as a function of $1/\sqrt{E}$. The (red) squares and the (blue) triangles represent the Čerenkov and scintillation channels, respectively. The Čerenkov data are well described by a straight line and the linear fit indicates that the constant term is almost 0. However, the resolution for the scintillation channel deviates from $1/\sqrt{E}$ scaling by 2 to 3% because of a response difference between

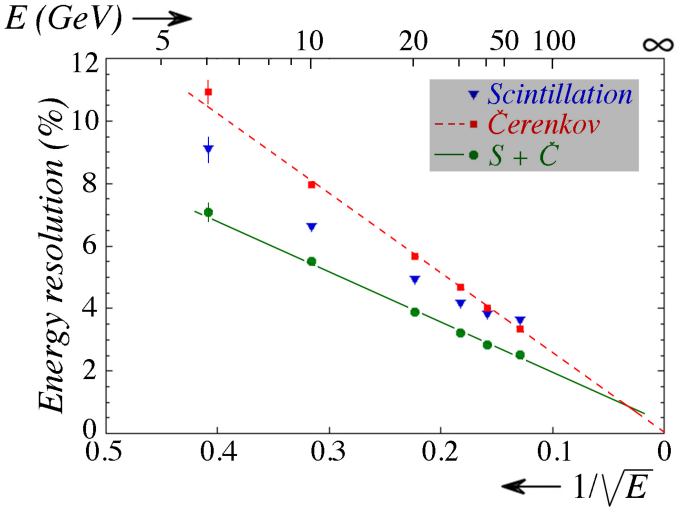

Fig. 4. The energy resolution for electrons in the Cu-fiber calorimeter as a function of $1/\sqrt{E}$. E is the beam energy.

particles entering the absorber material or the scintillating fibers. The (green) circles represent the resolution for the combined scintillation and Čerenkov signals. This resolution is indeed significantly better. The straight line fit corresponds to a stochastic term of 13.9% and a constant term of less than 1%.

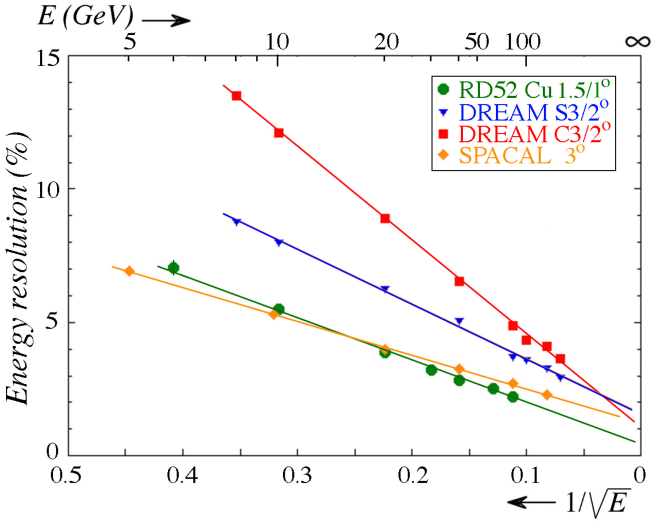

Fig. 5. Comparison of the energy resolutions for the RD52 Cu-fiber, original DREAM and SPACAL calorimeters.

In Fig. 5, the energy resolution of the combined signals is compared with the results reported for the original DREAM Cu-fiber calorimeter [1] and the SPACAL Pb-fiber calorimeter [2]. The RD52 calorimeter has substantially better energy resolution than the original DREAM calorimeter. At energies larger than 20 GeV, the em energy resolution is also better than for SPACAL.

B. The hadronic performance

The main goal of the Dual-REAdout Method (DREAM) calorimeter is to achieve high-precision energy measurements

for hadronic particles. This type of calorimeter offers the same advantages as compensating calorimeters, without the limitations of the latter, in terms of sampling fraction, signal integration time and volume, and the choice of absorber material. This is achieved by detecting both scintillation and Čerenkov signals simultaneously.

In the dual-readout method, the energy E of a hadron can be written as Eq. 1 [3], [4]:

$$E = \frac{S - \chi C}{1 - \chi} \quad \text{with} \quad \chi = \frac{1 - (h/e)_S}{1 - (h/e)_C} \tag{1}$$

The energy E is a function of the scintillation (S) and Čerenkov (C) signals measured for each event, χ is determined by the e/h values of the scintillating-fiber/absorber and Čerenkov-fiber/absorber structures. The Pb-fiber calorimeter was exposed to 20 GeV, 60 GeV and 100 GeV pions. Results are shown in Fig. 6.

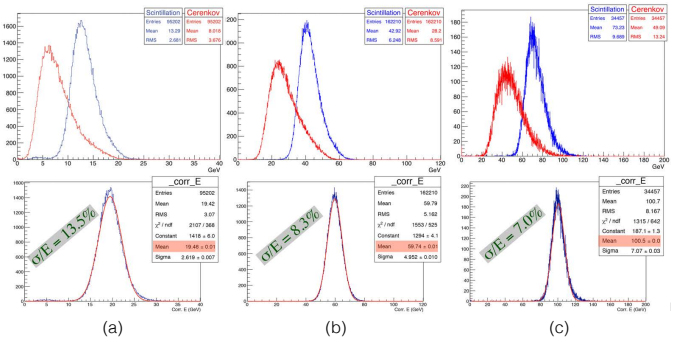

Fig. 6. Signal distributions of the scintillation and Čerenkov channels (upper), and the corrected energy E by the dual-readout method (lower) for 20 GeV (a), 60 GeV (b) and 100 GeV (c) pions. A value $\chi = 0.45$ was used to obtain the bottom row of plots.

The upper three plots of Fig. 6a, b and c are the signal distributions of the scintillation and Čerenkov channels for 20 GeV, 60 GeV and 100 GeV pions, respectively. They show the typical response function of non-compensating calorimeters, which are broad and asymmetric. Their mean values are lower than the incident beam energy. However, after applying Eq. 1, the signal distributions become more narrow and Gaussian, and center around the correct pion beam energy. This is shown in the bottom row of Fig. 6.

The hadronic energy resolutions obtained in this way were better than those obtained with the original DREAM calorimeter, but about 50% worse than those reported for SPACAL, the record holder in this field. The main reason for this is the limited size of our detector (1350 kg vs 20,000 kg for SPACAL). Lateral shower leakage is the dominant factor in the hadronic energy resolution of our calorimeter.

C. Particle identification

A longitudinally unsegmented calorimeter has several attractive features. First, this type of calorimeter doesn't need to have separate electromagnetic and hadronic sections. Thus, one can build a compact calorimeter system. Second, in a calorimeter system with separate electromagnetic and hadronic sections, hadrons deposit their energy in both sections. If these sections have different e/h values, intercalibration problems are inevitable. But this type of calorimeter has no intercalibration problem because of its longitudinally unsegmented structure. It is calibrated with electrons. The calibration process is very simple, since an em shower is almost entirely contained in one calorimeter tower. However, one may wonder how electromagnetic and hadronic particles can be identified in such a calorimeter. It turns out that there are several other shower features that may be used to identify particles, despite the absence of separate em and hadronic sections. Fig. 7 shows

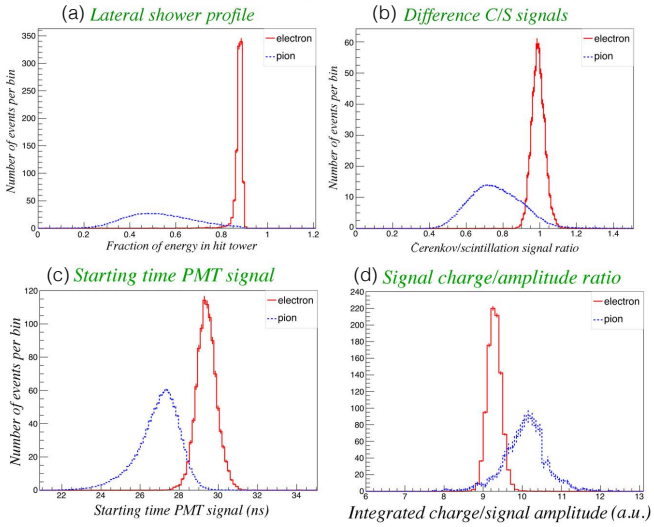

Fig. 7. The fraction of electron or pion energy deposited in the central tower (a). Distribution of the C/S signal ratio in the hit tower (b). Starting time of the scintillator signal (c). Ratio of the integrated charge to the amplitude of time structure (d).

the effects of these different features of the electromagnetic and hadron showers. Electrons deposit 85% of their entire energy in the hit tower of the RD52 calorimeter, while pions deposit typically 40-50% of their energy in that tower (Fig. 7a). Fig. 7b shows the effects of the C/S ratio. Showers initiated by electrons consist almost exclusively of relativistic particles (e^+,e^-). Hadron showers consist of electromagnetic and hadronic components. The hadronic component mostly consists of non-relativistic particles, while the electromagnetic component is relativistic. This electromagnetic component varies a lot in hadron showers. Therefore, Fig. 7b shows that the C/S signal ratio of pions fluctuates from 0.4 to 1, while that ratio is always close to 1.0 for em showers. The next different feature concerns the shower depth. On average, electrons produce light at a depth of 12 cm, and pions produce light at 60 cm inside the RD52 calorimeter. That corresponds to 10 X_0 and 2 λ_{int}, respectively. If we measure the time between the moment that a particle passes the trigger counters and the moment that a PMT signal is produced by the light generated in the fibers, electrons and hadrons have clearly different time distributions (Fig. 7c). We call this variable the starting time of the PMT signal. Finally, the ratio of the integrated charge and the amplitude of the PMT signal was used as a distinguishing variable. The time structure of the electron signals has always a similar width and amplitude, but

for hadron showers these characteristics fluctuate a lot. This is shown in Fig. 7d. When we identify electrons and pions using the lateral shower profile and the starting time of the PMT signal (which are uncorrelated), we could achieve 99% electron ID and 0.5% pion mis-ID.

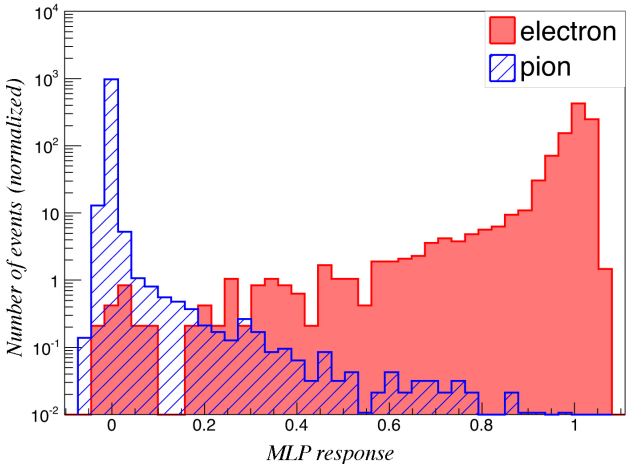

Fig. 8. Neural network responses to electrons and pions, when the neural network was trained with the variables from Fig. 7a, b and c.

We also trained a neural network with the lateral shower profile, the C/S ratio and the starting time of the PMT signal. Fig. 8 shows the responses of the neural network to electrons and pions. Most electrons populate the area near 1, while pions are near 0. Using the cut value 0.17, we could achieve 99.8% electron ID and 0.2% pion mis-ID efficiencies.

IV. Summary and Future Plans

We have shown several interesting experimental results based on the use of the Dual-REAdout Method principles. In the past year, two papers about the electromagnetic performance [5] and particle identification in the longitudinally unsegmentated calorimeter [6] were published. In addition, preliminary results on the hadronic performance were presented at the 2013 IEEE conference. In the future, we plan to build a larger detector to further improve the hadronic energy resolution. Also, we will test the possibility to separate 80 GeV from 90 GeV jets, i.e. the final state products of hadronically decaying W/Z bosons.

We used GEANT4 [7] to anticipate to what extent we can improve the hadronic energy resolution by building a larger detector. Three different sizes of the Cu-fiber calorimeters were simulated with GEANT4, and we investigated the energy resolution for 100 GeV pions in 3×3, 5×5 and 7×7 matrix detectors. This result is shown in Fig. 9a. The hadronic energy resolution improves from 7.5% for the 3×3 detector to 4.5% for the 7×7 detector.

For good physics results, excellent detector performance is essential. I expect that the Dual-REAdout Method calorimetry will open a new era of experimental possibilities in high energy particle physics, just as the high purity Germanium crystal detector opened a new era for nuclear physics.

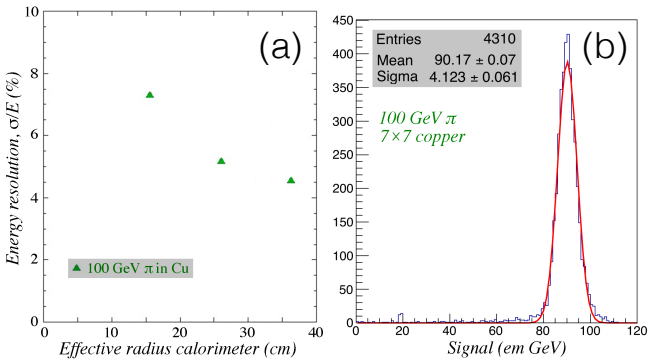

Fig. 9. The hadronic energy resolutions for 100 GeV π^- for the 3×3, 5×5 and 7×7 calorimeters based on the Cu-fiber structure predicted by GEANT4 (a). Signal distribution for 100 GeV pions in the 7×7 detectors after the dual-readout correction (b).

References

[1] N. Akchurin, et al., Nucl. Instr. and Meth. A 536 (2005) 29.
[2] D. Acosta, et al., Nucl. Instr. and Meth. A 308 (1991) 481.
[3] D.E. Groom, Nuclear Instruments and Methods in Physics Research A572 (2007) 633; A697 (2013) 84; A705 (2013) 24.
[4] R. Wigmans, New Journal of Physics 10 (2008) 025003.
[5] N. Akchurin, et al., Nucl. Instr. and Meth. in Phys. Res. A 735 (2014) 130.
[6] N. Akchurin, et al., Nucl. Instr. and Meth. in Phys. Res. A 735 (2014) 120.
[7] S. Agostinelli et al., Nucl. Instr. and Meth. in Phys. Res. A 506 (2003) 250.